Original Article

Concurrent vibration attenuation and low-power electricity generation in a locally resonant metastructure

Mohid Muneeb Khattak, Christopher Sugino and Alper Erturk

Abstract
We investigate piezoelectric energy harvesting on a locally resonant metamaterial beam for concurrent power generation and bandgap formation. The mechanical resonators (small beam attachments on the main beam structure) have piezoelectric elements which are connected to electrical loads to quantify their electrical output in the locally resonant bandgap neighborhood. Electromechanical model simulations are followed by detailed experiments on a beam setup with nine resonators. The main beam is excited by an electrodynamic shaker from its base over the frequency range of 0–150 Hz and the motion at the tip is measured using a laser Doppler vibrometer to extract its transmissibility frequency response. The formation of a locally resonant bandgap is confirmed and a resistor sweep is performed for the energy harvesters to capture the optimal power conditions. Individual power outputs of the harvester resonators are compared in terms of their percentage contribution to the total power output. Numerical and experimental analysis shows that, inside the locally resonant bandgap, most of the vibrational energy (and hence harvested energy) is localized near the excited base of the beam, and the majority of the total harvested power is extracted by the first few resonators.

Keywords
Metamaterials, metastructures, energy harvesting, piezoelectric, locally resonant

1. Introduction

Vibrational energy harvesting (VEH) is a concept wherein ambient vibrational energy is used to generate electricity to power small electronic components (Elvin and Erturk, 2013; Priya and Inman, 2009). This technique can replace or supplement conventional batteries, reducing the costs associated with accessing and replacing/recharging batteries for remote sensors. The direct piezoelectric effect refers to a phenomenon which converts mechanical strain into electricity. Piezoelectric energy harvesting (Anton and Sodano, 2007; Howells, 2009; Safaei et al., 2019) is a technique which uses this effect to harness vibrational energy from human motion, seismic activities, etc. and converts it into usable electrical power. Piezoelectric materials have high power density and they grant an ease of application due to which they are preferred over other conventional vibration energy conversion mechanisms such as electromagnetic (Glynne-Jones et al., 2004; Williams et al., 2001) and electrostatic (Mitcheson et al., 2004; Tvedt et al., 2010) techniques. Furthermore, piezoelectric harvesting devices are straightforward to manufacture in a multitude of configurations (Dutoit and Wardle, 2006; Erturk and Inman, 2011b; Roundy and

Wright, 2004), including microscale concepts and devices (Cook-Chennault et al., 2008). As this field continues to grow, researchers have introduced VEH capabilities to various types of vibrating structures (Safaei et al., 2019; Sugino and Erturk, 2018), such as linear cantilevers, bistable beams (Erturk and Inman, 2011a, 2011b) and plates (Arrieta et al., 2010), among others.

Metamaterials are architected structures that exhibit properties which are not readily found in ordinary materials, such as a negative refractive index (Zhu et al., 2014) and negative dynamic mass (Liu et al., 2000). Metamaterial-based finite structures with specified boundary conditions (i.e., metastructures), can exhibit the designed effective properties of the metamaterial provided a sufficient number of unit cells are used (Sugino et al., 2016, 2017a). Locally resonant

G.W. Woodruff School of Mechanical Engineering Georgia Institute of Technology, Atlanta, GA, USA

Corresponding author:
Christopher Sugino, G.W. Woodruff School of Mechanical Engineering, Georgia Institute of Technology, 801 Ferst Drive, Atlanta, GA 30332, USA.
Email: csugino3@gatech.edu
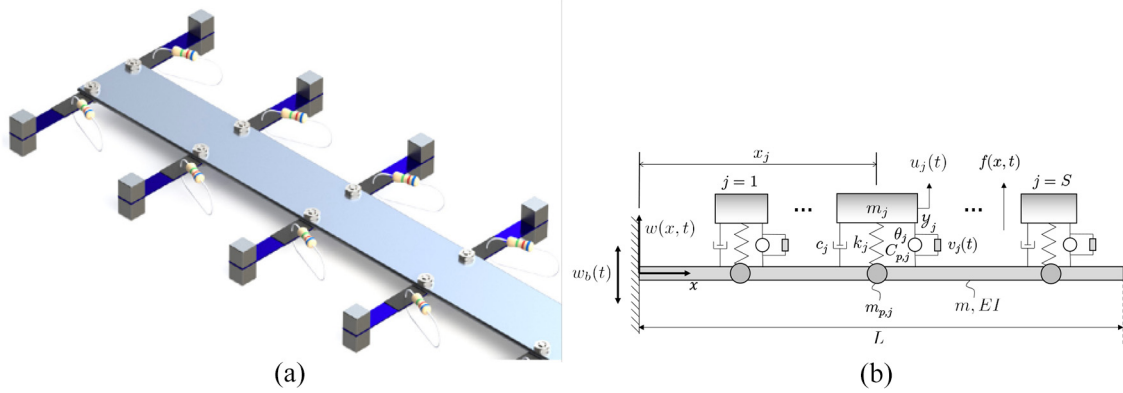
Figure 1. (a) Locally resonant energy harvesting metastructure with cantilever beams containing mechanical resonators and piezoelectric patches (Sugino and Erturk, 2018). (b) Schematic representation of the energy harvesting metastructure.

metastructures rely on an internal unit cell resonance to dramatically alter the effective properties of the metamaterial near the unit cell's resonant frequency (Ho et al., 2003; Liu et al., 2000; Patrick et al., 2021; Sugino and Erturk, 2018; Sugino et al., 2016; Wang et al., 2014, 2020). These systems can exhibit a locally resonant bandgap, or frequency range in which waves cannot propagate through the structure, at wavelengths much larger than the lattice size of the metamaterial. As a result, locally resonant metastructures have significant potential for low-frequency vibration attenuation.

An opportunity arises to explore multifunctional metastructures that not only allow for low-frequency vibration mitigation, but also have low-power VEH capabilities (Hu et al., 2018, 2021; Lan et al., 2021; Sugino and Erturk, 2018). Such VEH capabilities in a metamaterial could provide enough power for intermittent sensing, such as environmental monitoring or periodic diagnostic checks on the bandgap behavior of the structure. To that end, integrated energy harvesters could themselves be used as sensors/actuators for health monitoring. Furthermore, since locally resonant metamaterials already typically require bulky resonant elements, the barrier of entry for resonant piezoelectric energy harvesting is reduced.

This work numerically and experimentally investigates piezoelectric energy harvesting on a locally resonant metamaterial beam for concurrent power generation and bandgap formation. The first part of the paper reviews the governing equations (Sugino and Erturk, 2018) for the locally resonant energy harvesting metastructure along with the corresponding numerical results and experimental setup. Compared to previous investigations on such systems (Hu et al., 2018; Lan et al., 2021; Sugino and Erturk, 2018), the primary novelty of this work is the experimental characterization of a metamaterial with VEH capabilities and a locally resonant bandgap. Parameter identification for a single resonator is performed, and the identified

parameters are used to model the complete metastructure with nine pairs of piezoelectric energy harvester-resonators. Additionally, this work expands on previous work by numerically and experimentally characterizing the relative power contributed by the energy harvesters in the metastructure.

2. Locally resonant energy harvesting metastructure

2.1. Electromechanical model

We consider a locally resonant metastructure with attached piezoelectric energy harvesters, shown schematically in Figure 1. Following the analysis of Sugino and Erturk (2018), we have the following governing equation for the forced vibrations of a distributed parameter system:

$$
\mathcal{L}[w(\mathbf{P}, t)] + \left[m(\mathbf{P}) + \sum_{j=1}^{S} m_{p,j}\delta(\mathbf{P} - \mathbf{P}_j) \right] \ddot{w}(\mathbf{P}, t) -
$$
$$
\sum_{j=1}^{S} (k_j u_j(t) + c_j \dot{u}_j(t))\delta(\mathbf{P} - \mathbf{P}_j) = f(\mathbf{P}, t) \tag{1}
$$

Here $\mathcal{L}$ is the stiffness operator of order $2p$ where $p \geqslant 1$ defines the order of the system (Meirovitch, 1997; Sugino et al., 2017b), $w(\mathbf{P}, t)$ is the displacement of point $\mathbf{P}$ at time t where $\mathbf{P} \in D$, $m(\mathbf{P})$ is the host structure's mass distribution, $m_{p,j}$ is the mass of clamping hardware at attachment point $\mathbf{P}_j$, S is the number of resonators, $\delta(\mathbf{P})$ is the Dirac delta function, and $f(\mathbf{P}, t)$ is the external forcing. Note that mechanical damping will be introduced via modal damping at a later stage. For the system considered here, an Euler-Bernoulli beam model is used, corresponding to stiffness operator

$$
\mathcal{L} = \frac{\mathrm{d}^2}{\mathrm{d}x^2}\left(EI(x)\frac{\mathrm{d}^2}{\mathrm{d}x^2} \right) \tag{2}
$$

The corresponding energy harvester governing equations are as follows:

$$m_j\ddot{u}_j + c_j\dot{u}_j + k_ju_j - \theta_jv_j = -m_j\ddot{w}(\mathbf{P}_j, t) \quad (3)$$

$$C_{p,j}\dot{v}_j + \mathscr{Y}_j[v_j] + \theta_j\dot{u}_j = 0 \quad (4)$$

where k_j, c_j, m_j, u_j, and $\mathbf{P}_j$ are the stiffness, mechanical damping coefficient, mass, displacement, and position of the j th resonator respectively. θ_j, $C_{p,j}$, and $\mathscr{Y}_j$ are the electromechanical coupling, piezoelectric capacitance and admittance of the shunt circuit on the j th resonator.

Using a modal expansion procedure for the structure mode shapes without the resonators, we have the following approximate solution:

$$w(\mathbf{P}, t) = \sum_{r=1}^{N}\eta_r(t)\phi_r(P) \quad (5)$$

where N is the number of modes, ϕ_r is the rth mode shape of the plain structure, and η_r is the corresponding modal weighing. These mode shapes satisfy the orthogonality conditions given by:

$$\int_D m(\mathbf{P})\phi_r(\mathbf{P})\phi_s(\mathbf{P})dD = \delta_{rs} \quad (6)$$

$$\int_D \phi_r(\mathbf{P})\mathcal{L}[\phi_s(\mathbf{P})]dD = \omega_r^2\delta_{rs} \quad (7)$$

Here, ω_r is the natural frequency of the plain structure's rth mode shape. Substituting equation (5) into equation (1), multiplying by mode shape ϕ_k, integrating across the domain D and applying orthogonality conditions, we obtain the discretized governing equation

$$\left(\delta_{rk} + \sum_{k=1}^{N}\sum_{j=1}^{S}m_{p,j}\phi_r(\mathbf{P}_j)\phi_k(\mathbf{P}_j)\right)\ddot{\eta}_k + 2\zeta_r\omega_r\dot{\eta}_r +$$
$$\omega_r^2\eta_r - \sum_{j=1}^{S}(k_ju_j + c_j\dot{u}_j)\phi_r(\mathbf{P}_j) = q_r, \quad (8)$$

where ζ_r is the modal damping factor for the r th mode shape and

$$q_r(t) = \int_D \phi_r(\mathbf{P})f(\mathbf{P}, t)dD \quad (9)$$

Similarly, substituting equation (5) into equations (3) and (4) gives the discretized equations for the resonators:

$$m_j\ddot{u}_j + c_j\dot{u}_j + k_ju_j - \theta_jv_j = -m_j\sum_{r=1}^{N}\phi_r(\mathbf{P}_j)\ddot{\eta}_r \quad (10)$$

$$C_{p,j}\dot{v}_j + \mathscr{Y}_j[v_j] + \theta_j\dot{u}_j = 0 \quad (11)$$

Taking the Laplace transform of equations (8), (10), and (11), and rearranging, we have the following linear system of equations:

$$(s^2 + 2\zeta_r\omega_rs + \omega_r^2)H_r(s) +$$
$$s^2\left[m_j\frac{(2\zeta\omega_ts + \omega_t^2)}{s^2 + 2\zeta\omega_ts + \omega_t^2\left(1 + \frac{\gamma s}{s + h(s)}\right)} + m_{p,j}\right] \times \quad (12)$$
$$\sum_{k=1}^{N}H_k(s)\sum_{j=1}^{S}\phi_r(\mathbf{P}_j)\phi_k(\mathbf{P}_j) = Q_r(s)$$

where $H_r(s)$ and $Q_r(s)$ are the Laplace transforms of $\eta_r(t)$ and $q_r(t)$ respectively. For each resonator, $\omega_t^2 = \frac{k_j}{m_j}$ is the short-circuit resonant frequency and $\zeta = \frac{c_j}{2\omega_tm_j}$ is the damping ratio. Furthermore, $h(s) = \frac{Y_j(s)}{C_{p,j}}$ is the admittance of the shunt harvesting circuit ($Y_j(s)$ is the Laplace transform of $\mathscr{Y}_j$), and $\gamma = \frac{\theta_j^2}{k_jC_{p,j}}$ is the dimensionless coupling term. It is assumed that these normalized parameters are identical for each energy harvester, even if the mass m_j varies.

Both the energy harvester mass m_j and clamp mass $m_{p,j}$ are assumed to track the mass distribution of the host structure, that is,

$$m_j = \mu\left(m_{p,j} + m(\mathbf{P}_j)\Delta D_j\right) \quad (13)$$

$$m_{p,j} = \mu_pm(\mathbf{P}_j)\Delta D_j \quad (14)$$

where μ is the ratio of energy harvester mass to the host structure mass (including clamping hardware), and μ_p is the ratio of the clamp mass to the plain structure mass. With these substitutions, equation (12) becomes

$$(s^2 + 2\zeta_r\omega_rs + \omega_r^2)H_r(s) +$$
$$s^2\left[\mu(1 + \mu_p)\frac{(2\zeta\omega_ts + \omega_t^2)}{s^2 + 2\zeta\omega_ts + \omega_t^2\left(1 + \frac{\gamma s}{s + h(s)}\right)} + \mu_p\right] \times$$
$$\sum_{k=1}^{N}H_k(s)\sum_{j=1}^{S}m(\mathbf{P}_j)\phi_r(\mathbf{P}_j)\phi_k(\mathbf{P}_j)\Delta D_j = Q_r(s)$$
$$(15)$$

The form of equation (15) highlights the metastructure behavior as the number of unit cells in becomes large (see e.g. Sugino and Erturk, 2018; Sugino et al., 2017a), since

$$\lim_{S\to\infty}\sum_{j=1}^{S}m(\mathbf{P}_j)\phi_r(\mathbf{P}_j)\phi_k(\mathbf{P}_j)\Delta D_j =$$
$$\int_D m(\mathbf{P})\phi_r(\mathbf{P})\phi_k(\mathbf{P})dD = \delta_{rk} \quad (16)$$

yielding the simplification
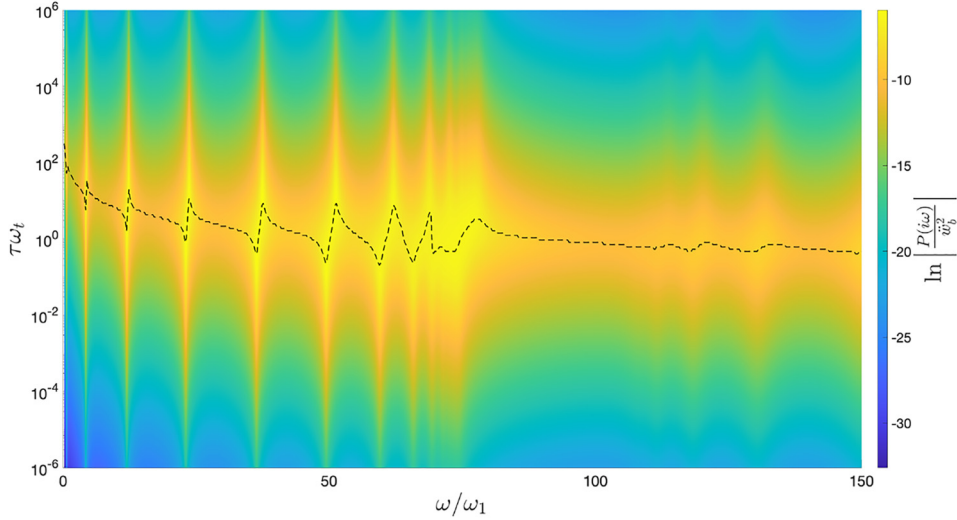
Figure 2. Optimal total power of the metastructure ($S = 20$ resonators) versus normalized excitation frequency (ω/ω_1) and normalized resistive load ($\tau\omega_t$) at $\omega_t/\omega_1 = 75$.

$$[s^2(1 + \mu_p)\left(1 + \frac{\mu(2\zeta\omega_t s + \omega_t^2)}{s^2 + 2\zeta\omega_t s + \omega_t^2\left(1 + \frac{\gamma s}{s + h(s)}\right)}\right) +$$
$$2\zeta\omega_r s + \omega_r^2]H_r(s) = Q_r(s)$$

(17)

assuming a sufficient number of resonators are used. Equation (17) shows that presence of energy harvesters on the metastructure results in effective mass that varies with frequency, that is,

$$\frac{\hat{M}(s)}{M_p} = (1 + \mu_p)\left(1 + \frac{\mu(2\zeta\omega_t s + \omega_t^2)}{s^2 + 2\zeta\omega_t s + \omega_t^2\left(1 + \frac{\gamma s}{s + h(s)}\right)}\right)$$

(18)

where the factor $(1 + \mu_p)$ indicates that the point masses simply add to the primary structure mass, without the frequency dependence. The locally resonant bandgap appears when the effective mass becomes negative. For a metastructure with light damping ($\zeta\approx0$) and small piezoelectric coupling ($\gamma\approx0$), the locally resonant bandgap appears in the frequency range $\omega_t < \omega < \omega_t\sqrt{1 + \mu}$.

Equation (12) is used in the next section to obtain numerical results for the locally resonant bandgap and useful power output corresponding to the model in Figure 1.

2.2. Numerical results

For the numerical simulations, we consider an aluminum beam with $S = 20$ harvesters at a target frequency ratio $\frac{\omega_t}{\omega_1} = 75$. The beam is clamped at one end ($x = 0$) and vibrates freely at the other end ($x = L$). It has width w, thickness h, and length L. The beam has a mass density of ρ and a Young's modulus of E. It has a mass per length of m_b. The mass ratios for the simulated system are $\mu_p = 0$ and $\mu = 1$.

We consider purely resistive shunt circuits to quantify the power output of the energy harvesters, corresponding to normalized shunt admittance $h(i\omega) = \frac{1}{\tau}$, where $\tau = RC_{p,j}$ is the circuit time constant and R is the load resistance. At each frequency of excitation, the optimal load τ_{opt} that gives the maximum power output from the full metastructure is obtained. Figure 2 shows the total optimal real power output of the mechanical metastructure versus normalized resistive load and frequency with 20 harvesters. The maximum broadband power output occurs near the resonant frequency $\frac{\omega_t}{\omega_1} = 75$, immediately before the resonant bandgap. The dashed line here shows optimal loading at each excitation frequency. Figure 3 shows the tip transmissibility at the optimal loading τ_{opt}, showing that the locally resonant bandgap is present even when the maximum electrical power is harvested from the metastructure.

For the same model, the power output for individual harvesters at the optimal load for the full metastructure was plotted to identify the harvesters which output the maximum power. Figure 4 shows that the harvesters near the excited base yield significantly more power than those far from the excitation, especially inside the locally resonant bandgap.

The effect of optimal power as we move along the beam from the first harvester toward the last can be seen in Figure 5(a) (as an absolute quantity) and Figure 5(b) (as a percentage of the total) for various target frequencies ($\omega_t/\omega_1 = 25, 50, 75,$ and 100). After the first 10 harvesters, the power output is significantly reduced. Targeting a lower vibration mode neighborhood results
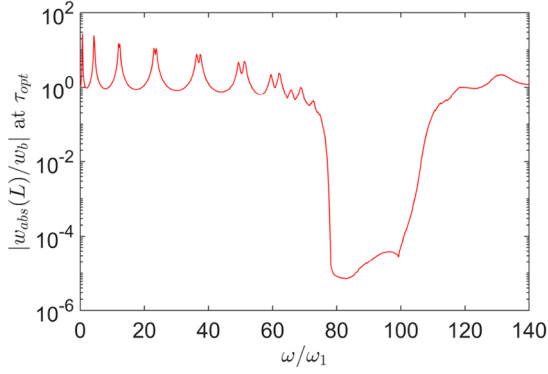
Figure 3. Tip transmissibility versus normalized excitation frequency at the optimal normalized resistive load τ_{opt} for $\frac{\omega_t}{\omega_1}$=75 with 20 harvesters.

in higher power output; however, the trend of decreasing power farther from the excitation point is similar. The first two harvesters are responsible for 65% and 22% of the total power contribution for each case of normalized frequency.

3. Experimental results

The experimental system under consideration comprises a main beam with nine cantilever attachments. Each small cantilever beam comprises two identical mechanical resonators with tip masses. Piezoelectric

patches are bonded at the base of each cantilever on both sides of the main beam and connected to electrical loads (resistors) to quantify the electrical output from these sensors in the locally resonant bandgap neighborhood. The main beam is excited using an electrodynamic shaker within the frequency range of 0–150 Hz and the corresponding tip displacement is measured via a laser Doppler vibrometer (LDV) which measures the transmissibility frequency response. The voltage output from each piezoelectric element is also measured to quantify the energy harvesting capabilities of the metamaterial. A resistance sweep is performed after bandgap confirmation to obtain the optimal electrical load for maximum power output. The experimental setup is shown in Figure 6.

3.1. Single energy harvester characterization

To estimate parameters for the full locally resonant metastructure, a single energy harvester was isolated from the full structure as shown in Figure 7. Experiments were performed by mounting the cantilever to an electrodynamic shaker for base excitation. An accelerometer was mounted to the shaker to measure input acceleration while the tip velocity of the cantilever was measured using an LDV. The voltage output from the piezoelectric patch (across each load resistance) was also measured during experiments.

Model parameters for the lumped-element model (equations (3) and (4)) were obtained from the
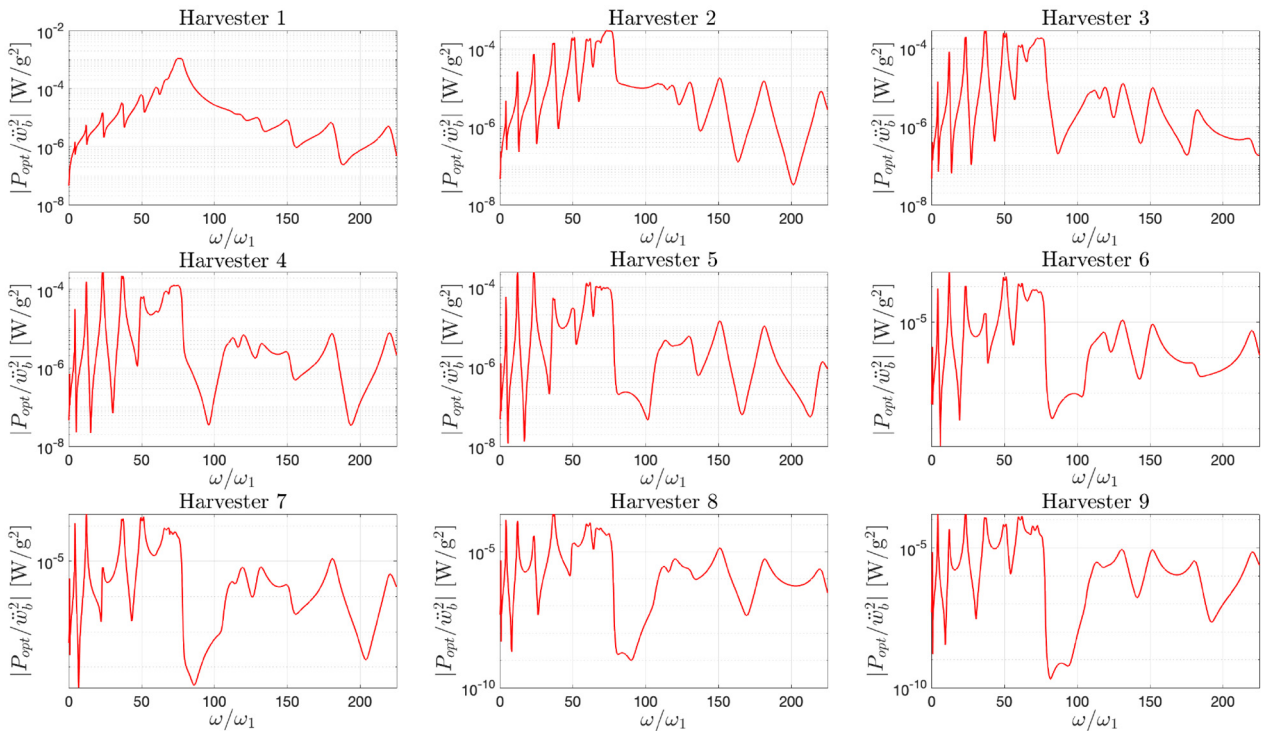
Figure 4. Optimal power output versus normalized excitation frequency for the first nine harvesters at $\frac{\omega_t}{\omega_1}$=75.
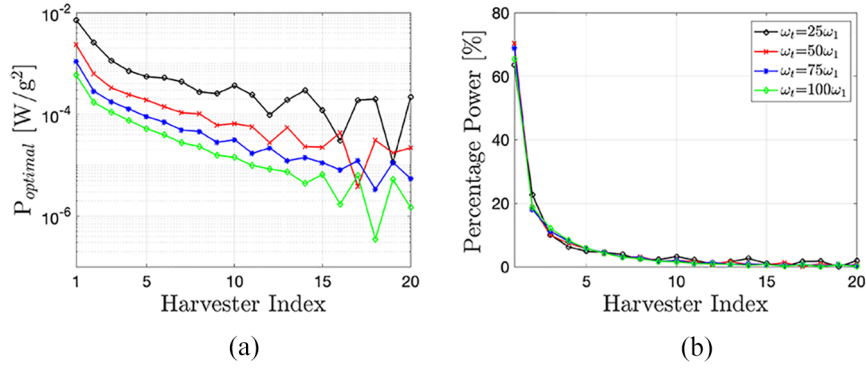
Figure 5. (a). Optimal power versus harvester index and (b) percentage power contribution as a function of harvester index.

1	Main beam
2	Resonator
3	Piezo patch
4	Accelerometer
5	Electrodynamic shaker
6	Resistors
7	Data acquisition device
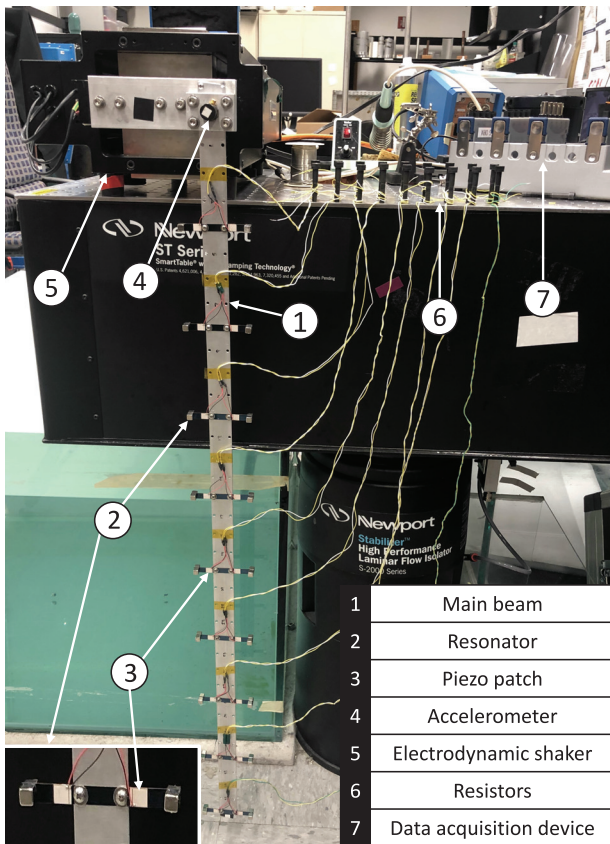
Figure 6. Experimental setup consisting of the main beam with nine piezoelectric energy harvester-resonators attached to electrical loads.

experimental FRFs. The lumped mass m was approximated as the mass of the magnets placed on the tip of the cantilever, since the tip mass was much greater than the cantilever mass. The mechanical damping coefficient was measured using the experimental FRFs via the quality factor (Q) given as:

$$Q = \frac{f_r}{\Delta f} \tag{19}$$
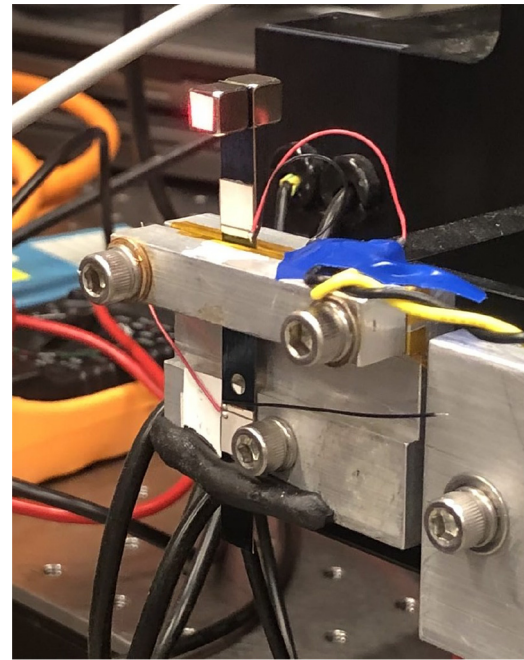
Figure 7. Single isolated resonator setup clamped to the shaker.

where f_r is the resonant frequency and Δf is the half-power bandwidth corresponding to short circuit (SC) or open circuit (OC) half-power points $\left(f_{SC,OC} = \frac{|TR|_{SC,OC}}{\sqrt{2}} \right)$. The corresponding damping ratio ζ and the damping coefficient were then calculated as

$$\zeta = \frac{1}{2Q} \tag{20}$$

$$c = 2\zeta\sqrt{mk} \tag{21}$$

The equivalent stiffness k was estimated using the experimental SC resonant frequency f_{SC} as

$$k = (2\pi f_{SC})^2 m \tag{22}$$

Table 1. Estimated parameters for the single resonator.

m– resonator tip mass	0.0036 kg
c– mechanical damping coefficient	0.0525 N/m/s
k– spring steel stiffness	853.63 N/m
θ– electromechanical coupling	-1.8884×10^{-4} N/V
C_p– capacitance	3.23×10^{-9} F

Table 2. Parameters used for the modeled system.

m– resonator tip mass	0.0036 kg
c– mechanical damping coefficient	0.0525 N/m/s
k– spring steel stiffness	853.63 N/m
θ– electromechanical coupling	-1.8884×10^{-4} N/V
C_p– capacitance	3.23×10^{-9} F
E– Young's modulus	70×10^9 Pa
w– width of the beam	0.0254 m
h– thickness of the beam	1.49×10^{-3} m
ρ– density	2700 kg/m^3
L– length of beam	0.9144 m
m_b– mass per length of beam	0.0985 kg/m
m_c– mass of clamps	0.0017 kg
ω_1– fundamental frequency	9.236 rad/s

Using the OC resonant frequency f_{OC}, the electromechanical coupling θ was calculated as

$$\theta = \sqrt{C_p(m2\pi f_{OC}^2 - k)} \qquad (23)$$

where C_p is the measured capacitance of the piezoelectric unit cell attached to the spring steel cantilever. The experimental results are shown in Figure 8, and the experimentally identified parameters are shown in Table 1. Overall, there is excellent agreement between the model and experimental results. The single harvester's resonant frequency exhibits a clear shift from SC ($R_l \to 0$) to OC ($R_l \to \infty$) conditions. As load resistance is increased from SC to OC, the power output (Figure 8(c)) approaches a maximum value (Erturk and Inman, 2008) at the optimal load of 887 kΩ ($f = 77.8$ Hz).

3.2. Energy harvesting metastructure

Following the single resonator parameter identification case, experimental results were obtained for the complete metastructure for all load resistances as shown in Figure 6. Transmissibility and power FRFs were plotted for each resistance value and optimal loading was identified. It was then compared with the modeled system as described in previous section using the individual harvester parameters in Table 1 and primary
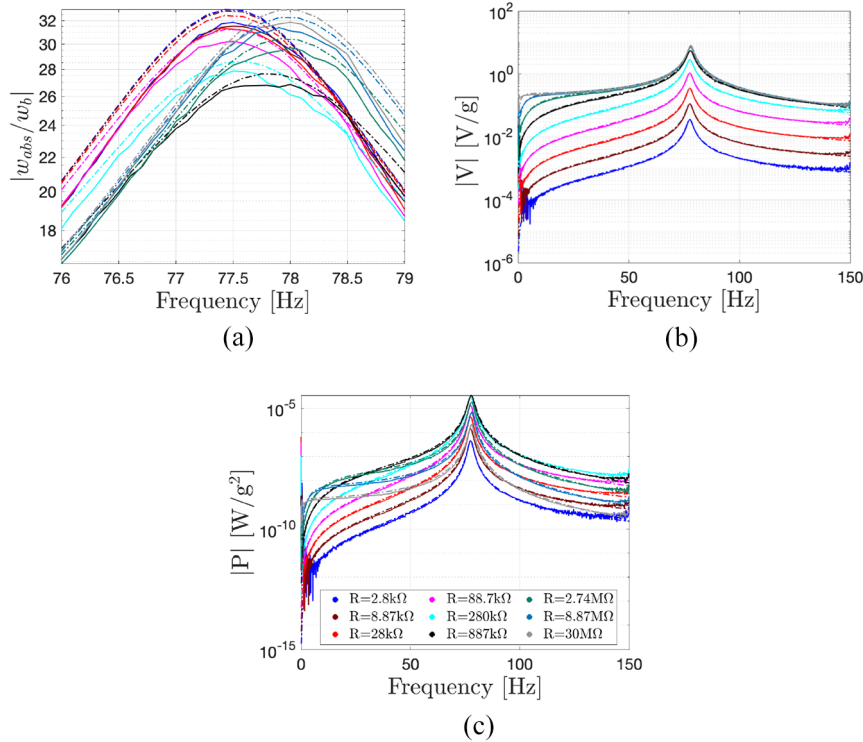
Figure 8. (a) Transmissibility comparison at all resistances for the single harvester, (b) voltage output comparison at all resistances for the single harvester, and (c) power output comparison at all resistances for the single harvester. Dashed line in the figures corresponds to the model whereas solid line represents experimental data.
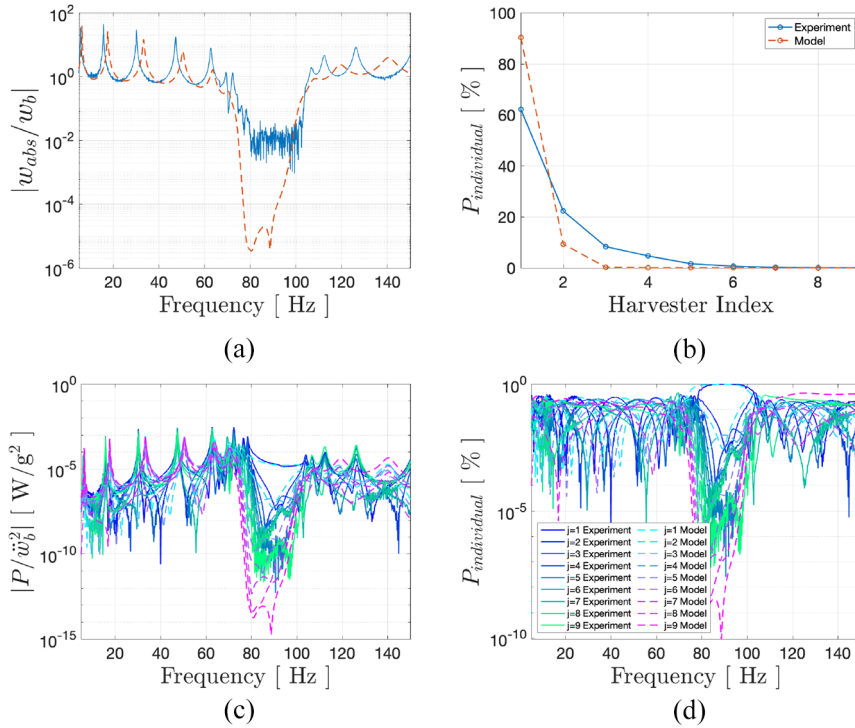
Figure 9. (a) Transmissibility comparison versus frequency, (b) fractional power contribution comparison as a function of harvester index at 80 Hz, (c) power output comparison of each harvester, and (d) fractional power contribution comparison versus frequency. All comparison between experimental and model data has been done at $R_l = 280$ kΩ.

beam parameters summarized in Table 2 . For the sake of brevity, model and experimental data comparison has only been shown for a load resistance of 280 kΩ, which yielded the maximum power output among all load resistances that were tested. The experimental and model tip transmissibility, power output, and percentage power contribution are shown in Figure 9. Note that the optimal load for the full metastructure does not match the optimal load for the single harvester 887 kΩ, but 280 kΩ gave nearly identical power output for the single harvester (see Figure 8(c)). Thus, the difference in optimal load can be attributed to the small variation of energy harvester properties in the metastructure.

Figure 9 shows that the model matches well with the experimental data. The tip transmissibility in Figure 8 shows that a locally resonant bandgap was created in the system. The discrepancies between the model and experimental results can be attributed to the variation in unit cell properties, the use of a simplified model for each energy harvester, and the influence of each resonator's clamping hardware. The experimental results show that the use of resonant energy harvesters can generate useful power while still achieving significant vibration attenuation through the formation of a locally resonant

bandgap. This result is promising for the development of metastructures with integrated energy harvesting capabilities, increasing their multifunctionality. For example, this concept could be used for integrated low-power sensors and devices for intermittent self-sensing and diagnostics.

For the individual power contribution by each harvester, it can be seen in Figure 9(c) and (d) that the harvester closest to the base contributes the most power, especially inside the locally resonant bandgap. These results confirm that inside the locally resonant bandgap, most of the vibrational energy (and the corresponding useful energy harvested) is concentrated near the base of the beam, gradually decreasing toward the tip of the structure. Furthermore, this power output is concentrated and maximum right at the start of the bandgap at the resonant frequency of the energy harvesters. Importantly, this suggests that it may not be necessary to use energy harvesters in every unit cell of the metastructure, provided that the excitation source is consistent. This would greatly reduce the complexity of the energy harvesting metastructure, without significantly compromising its bandgap attenuation performance. At the same time, some care must be taken if the unit cells of the metamaterial are not identical to

ensure that the locally resonant bandgap forms as expected. This may not be a concern for a metamaterial with weakly-coupled piezoelectric energy harvesters (i.e. small γ), but very well-coupled energy harvesters may introduce significant damping to the metamaterial that should be accounted for.

4. Conclusions

This paper presents the numerical and experimental analysis of a energy-harvesting locally resonant (LR) metastructure. A modal analysis procedure is used to discretize the governing equations for the structure, yielding both finite metastructure response and the infinite metamaterial-type effective properties. Simulations demonstrate that most of the useful power output of these metastructures is obtained by the harvesters closest to the excitation. An experimental platform was developed comprising a primary cantilever beam with attached cantilever-type piezoelectric energy harvesters with tip masses. Experimental model parameters were obtained for a single energy harvester and then extended to the full metastructure with nine pairs of energy harvesters. The experimental results show good agreement to the model predictions, validating the overall model approach. Additionally, the experimental results confirm that most of the harvested power comes from the first few energy harvesters closest to the excitation, suggesting that it may be sufficient to use only a few energy harvesters in such LR metastructures. Future research could be extended to LR metastructures with nonlinear energy harvesters to obtain better attenuation performance and increase the bandwidth of energy harvesting.

Declaration of conflicting interests

Funding

ORCID iDs

Christopher Sugino https://orcid.org/0000-0001-7547-4874
Alper Erturk https://orcid.org/0000-0003-0110-5376

References

Anton SR and Sodano HA (2007) A review of power harvesting using piezoelectric materials (2003–2006). *Smart Materials and Structures* 16(3): R1–R21.

Arrieta AF, Hagedorn P, Erturk A, et al. (2010) A piezoelectric bistable plate for nonlinear broadband energy harvesting. *Applied Physics Letters* 97(10): 104102.

Cook-Chennault KA, Thambi N and Sastry AM (2008) Powering MEMS portable devices—a review of non-regenerative and regenerative power supply systems with special emphasis on piezoelectric energy harvesting systems. *Smart Materials and Structures* 17(4): 043001.

Dutoit NE and Wardle BL (2006) Performance of microfabricated piezoelectric vibration energy harvesters. *Integrated Ferroelectrics* 83(1): 13–32.

Elvin N and Erturk A (2013) *Advances in Energy Harvesting Methods*. New York, NY: Springer Science & Business Media.

Erturk A and Inman D (2011b) *Piezoelectric Energy Harvesting*. New York, NY: John Wiley & Sons, Ltd.

Erturk A and Inman DJ (2008) A distributed parameter electromechanical model for cantilevered piezoelectric energy harvesters. *Journal of Vibration and Acoustics* 130: 041002.

Erturk A and Inman DJ (2011a) Broadband piezoelectric power generation on high-energy orbits of the bistable duffing oscillator with electromechanical coupling. *Journal of Sound and Vibration* 330(10): 2339–2353.

Glynne-Jones P, Tudor MJ, Beeby SP, et al. (2004) An electromagnetic, vibration-powered generator for intelligent sensor systems. *Sensors and Actuators A Physical* 110(1–3): 344–349.

Ho KM, Cheng CK, Yang Z, et al. (2003) Broadband locally resonant sonic shields. *Applied Physics Letters* 83(26): 5566–5568.

Howells CA (2009) Piezoelectric energy harvesting. *Energy Conversion and Management* 50(7): 1847–1850.

Hu G, Tang L and Das R (2018) Internally coupled metamaterial beam for simultaneous vibration suppression and low frequency energy harvesting. *Journal of Applied Physics* 123(5): 055107.

Hu G, Tang L, Liang J, et al. (2021) Acoustic-elastic metamaterials and phononic crystals for energy harvesting: A review. *Smart Materials and Structures* 30: 085025.

Lan C, Hu G, Tang L, et al. (2021) Energy localization and topological protection of a locally resonant topological metamaterial for robust vibration energy harvesting. *Journal of Applied Physics* 129(18): 184502.

Liu Z, Zhang X, Mao Y, et al. (2000) Locally resonant sonic materials. *Science* 289(5485): 1734–1736.

Meirovitch L (1997) *Principles and Techniques of Vibrations*. Upper Saddle River, NJ: Prentice Hall.

Mitcheson PD, Miao P, Stark BH, et al. (2004) Mems electrostatic micropower generator for low frequency operation. *Sensors and Actuators A Physical* 115(2–3): 523–529.

Patrick J, Adhikari S and Hussein MI (2021) Brillouin-zone characterization of piezoelectric material intrinsic energy-harvesting availability. *Smart Materials and Structures* 30: 085022.

Priya S and Inman DJ (2009) *Energy Harvesting Technologies*, vol. 21. New York, NY: Springer.

Roundy S and Wright PK (2004) A piezoelectric vibration based generator for wireless electronics. *Smart Materials and Structures* 13(5): 1131–1142.

Safaei M, Sodano HA and Anton SR (2019) A review of energy harvesting using piezoelectric materials: State-of-the-art a decade later (2008–2018). *Smart Materials and Structures* 28(11): 113001.

Sugino C, Leadenham S, Ruzzene M, et al. (2017a) An investigation of electroelastic bandgap formation in locally

resonant piezoelectric metastructures. *Smart Materials and Structures* 26(5): 055029.

Sugino C, Xia Y, Leadenham S, et al. (2017b) A general theory for bandgap estimation in locally resonant metastructures. *Journal of Sound and Vibration* 406: 104–123.

Sugino C and Erturk A (2018) Analysis of multifunctional piezoelectric metastructures for low-frequency bandgap formation and energy harvesting. *Journal of Physics D Applied Physics* 51(21): 215103.

Sugino C, Leadenham S, Ruzzene M, et al. (2016) On the mechanism of bandgap formation in locally resonant finite elastic metamaterials. *Journal of Applied Physics* 120(13): 134501.

Tvedt LGW, Nguyen DS and Halvorsen E (2010) Nonlinear behavior of an electrostatic energy harvester under wide-and narrowband excitation. *Journal of Microelectromechanical Systems* 19(2): 305–316.

Wang P, Casadei F, Shan S, et al. (2014) Harnessing buckling to design tunable locally resonant acoustic metamaterials. *Physical Review Letters* 113(1): 014301.

Wang YF, Wang YZ, Wu B, et al. (2020) Tunable and active phononic crystals and metamaterials. *Applied Mechanics Reviews* 72(4): 040801.

Williams CB, Shearwood C, Harradine MA, et al. (2001) Development of an electromagnetic micro-generator. *IEE Proceedings - Circuits Devices and Systems* 148(6): 337–342.

Zhu R, Liu XN, Hu GK, et al. (2014) Negative refraction of elastic waves at the deep-subwavelength scale in a single-phase metamaterial. *Nature Communications* 5: 5510.